Biomass Conversion and Biorefinery (2024) 14:2529–2542
https://doi.org/10.1007/s13399-022-02709-5

ORIGINAL ARTICLE

Activated eco-waste of *Posidonia oceanica* rhizome as a potential adsorbent of methylene blue from saline water

Randa R. Elmorsi[1] · Khaled S. Abou-El-Sherbini[2] · Waleed A. Shehab El-Dein[3] · Hesham R. Lotfy[4]

Received: 28 November 2021 / Revised: 15 April 2022 / Accepted: 19 April 2022 / Published online: 6 May 2022

Abstract

A new activated adsorbent was produced from the debris of *Posidonia oceanica rhizomes* (POR). POR were activated in acetic acid and utilized as an eco-adsorbent for the removal of cationic dye methylene blue (MB) from saline solutions. The purified *Posidonia oceanica rhizomes* (PPOR) and its activated form (APOR) were characterized by elemental analysis, pH-metric titration, Fourier transformer infrared (FTIR), and surface area measurements, which inferred a remarkable activation of APOR. An enhancement in the free acidic sites was confirmed. The adsorption data obtained were analyzed using Langmuir, Freundlich, Temkin, Dubinin-Kaganer-Raduskavich (DKR), and Redlich and Peterson (RP) isotherm models. The obtained data from these isotherm models were tested using some error functions (residual root mean squares error (RMSE), sum square error (SSE), and chi-square test (X^2) function). Temkin isotherm model was the best isotherm fits the experimental data of APOR. Kinetic data were evaluated by pseudo-first-order (PFO), pseudo-second-order (PSO), and intraparticle diffusion models. The adsorption rate was found to follow PSO model with a good correlation ($R^2 = 0.999–1$). A suggested, endothermic, multilayer, combined electrostatic and physical adsorption mechanism may be responsible for the removal of MB from water utilizing APOR. Adsorption is anticipated to start with chemisorption on active functional groups of adsorbent's surface followed by physisorption of the subsequent layers through adsorbate–adsorbate interaction. The removal process was successfully applied for MB-spiked saline and brackish water with removal efficiencies of 51.7–97.2%. The results revealed that activated *Posidonia oceanica rhizomes* is a promising adsorbent for the removal of the methylene blue dye from real saline and brackish water with high removal efficiencies.

Keywords *Posidonia oceanica rhizome* debris · Acid activation · Methylene blue · Adsorption · Contaminated saline water

✉ Hesham R. Lotfy
heshamrabielotfy@yahoo.com;
hesham.rabie@deltauniv.edu.eg

Randa R. Elmorsi
rrelmorsi@hotmail.com

Khaled S. Abou-El-Sherbini
kh_sherbini@yahoo.com

Waleed A. Shehab El-Dein
waleedazmy1967@yahoo.com

[1] Laboratory of Marine Chemistry, National Institute of Oceanography and Fisheries, NIOF, Cairo, Egypt

[2] Department of Inorganic Chemistry, National Research Centre, 33 El Bohouth St. (Former Eltahrir St.), P.O. 12622, Dokki, Giza, Egypt

[3] Department of Mathematics & Engineering Physics, Faculty of Engineering, Mansoura University, El-Mansoura, Egypt

[4] Basic Sciences Department, Faculty of Engineering, Delta University for Science and Technology, Coastal High Way, Gamasa, Al-Dakahlia, Egypt

1 Introduction

Water scarcity is one of the most serious crises facing the world currently so it is necessary to make effective utilization of the available water resources. Environmental pollution is in an alarming problem which is facing the world due to industrialization and urbanization. Industrial wastewater discharge is causing severe pollution in the environment and has become a challenge for scientists and researchers. Various dye effluents from pickling industries, paper, dyestuff industries, tanning, and textile industries are polluting limited water resources when discharged without proper treatment [1]. Dyeing effluents are hazard-rich, which inflict acute disorders in the aquatic ecosystem such as high chemical oxygen demand (COD) and an increase in toxicity. Also, the colored wastewater harms the esthetic nature of water and affects the light permeability of the water's surface and the photosynthetic activity of the aquatic organisms

[2]. Many of the dyes used in these industries may also be carcinogenic and mutagenic. The aromatic nature of most synthetic dyes makes them very stable and resistant to biodegradation and photo-degradation, which result in long-lasting water pollution [1, 2].

In recent years, research is focusing on the utilization of appropriate, low-cost green technology for the pre-treatment of wastewater discharges [3–5]. Different processes for removing residual dyes typically include physicochemical [5–13], catalytic processes [14, 15], electrochemical [7, 8, 14, 16], magnetically assisted processes [, 14, 15], and biological [17–19] schemes. Some processes such as electrochemical techniques are relatively new for textile waste treatment, while bio-treatment and adsorption in particular [3, 9, 20, 21] are applicable in the industry because they are simple, regenerative, and fast techniques. Promising adsorbents are lingo cellulosic agricultural by-products and eco-wastes [3, 22–26] because of their low cost, high adsorption capacity, porous structure, and large surface area that is rich with versatile acidic and basic sites and at the same time, waste re-use represents one of the pillars of the circular economy philosophy [4]. They have been proven to remove dyes and other pollutants from aqueous environments. However, cheap and efficient adsorbents in the presence of a saline background are relatively rare due to the competition of matrix ions [3, 27].

Posidonia oceanica (PO) is an endemic dominant seagrass (SG), which covers approximately 50,000 km^2 of the total coastal sandy regions in the Mediterranean Sea and contributes to the seawater oxygenation and cleaning, fauna protection, and littoral erosion prevention [28, 29]. *P. oceanica* is viewed as a pollution-biomonitor since it naturally retrieves heavy metal ions from seawater in its living organs, such as its leaves, holding various amounts of heavy metal ions, from a small mg kg^{-1} of As, Cd, and Pb up to several tens of mg kg^{-1} of Zn [30–33]. The aggregated dead SG (called aegagropiles) form large wastes along the Mediterranean shore, thus imposing an environmental risk [29, 34]. These dead wastes are a natural cation-exchanger lignocellulosic framework, which is adapted to highly saline environments [34]. Hence, they were directly utilized (or after modification) as a bio-adsorbent for MB [35, 36] and Pb^{2+} ions [37, 38] from wastewater. The Mediterranean aegagropiles are either ellipsoidal (egg-shaped; major) or spherical in shape (ball-shaped; minor). The ellipsoidal shape includes almost 60% of the cases with the heterogeneous type of aegagropiles, i.e., containing a rhizomatic nucleus, whereas all of the spherical aegagropiles are of the homogeneous or intermediate type [39]. The rhizomes constitute 35% on average of *P. oceanica plant* [30]. Despite the environmental importance of *P. oceanica* rhizomes (POR) as a natural remediation tool, its waste is imposing an environmental problem and was not studied as adsorbent. The current study introduces a simple and new acid-activation method for the recycling of POR eco-waste as an environmental friendly adsorbent for methylene blue as a model for cationic dyes from saline water.

2 Experimental

2.1 Materials

Commercial glacial acetic acid was purchased from Doummar & Sons Co. (Adra, Syria). MB chloride hydrate (3,7-bis(dimethylamino)-phenothiazin-5-ium chloride, $C_{16}H_{18}ClN_3S{\cdot}xH_2O > 96.0\%$) was purchased from S D Fine-Chem Limited (Mumbai, India). Stock solutions (1000 mg L^{-1}) were prepared by dissolving 1 g of MB in 1 l of distilled water (DW). Other chemicals and reagents were of grade Puriss from Sigma–Aldrich unless otherwise stated.

POR debris were collected from the shores of Marsa Matruh, Egypt, washed thoroughly with tap water, skimmed, dried in the air, and coded as POR_{raw}. To examine the practical application, surface water samples were collected from different sites along the coasts of northeast Egypt, Hurghada, Burullus, and Manzala lakes, which represent different salinity degrees.

2.2 Equipments

Inductively coupled plasma–optical emission spectroscopy (ICP-OES) was performed on an iCAP-7000 SERIES ICP Spectrometer, Thermo-Fisher Scientific, Germany, to determine the elements Li, K, Mg, Ca, Sr, Ba, B, Al, Cr, Mn, Fe, Co, Cu, Zn, and Cd concentrations in digested samples of PORs. The plant debris samples were digested in a microwave oven from MILESTONECONNECT model ETHOS EASY using 0.5 g of each sample in 8 mL concentrated HNO_3 and 2 mL concentrated H_2O_2. Single element stock standards (Fisher Scientific) were used to prepare multi-element standard solutions with the necessary element concentrations. The standard solutions were used for calibration curve generation. An automatic Vario EL, Elementar instrument, Germany, was used to determine the percentage of C, H, N, and S in the samples. Nitrogen adsorption/desorption isotherms were performed to determine the surface texture parameters at liquid nitrogen temperature (− 196 °C) using Quantachrome Nova 3200 S automates gas sorption apparatus (USA). Before such measurements, samples were perfectly degassed at 70 °C for 4 h under vacuum pressure 5×10^{-4} Pa. Fourier transform infrared (FTIR) spectra were recorded on a Nicolet iS10 instrument, Thermo-Fisher Scientific, USA, using KBr pellets. The pH of each sample solution was adjusted with NaOH and H_2SO_4 solutions using a Cole-Parmer Chemcadet 5986–50 pH/ion/mV meter, USA, with an expanded range and an accuracy of ± 0.1.

The pH-metric titration measurement was performed using a Metrohm 848 Titrino automatic potentiometer, Switzerland. One hundred milligram portion of the investigated sample was added to 25 mL of 0.5 mol L^{-1} KCl and titrated against 0.0073 mol L^{-1} KOH + 0.5 mol L^{-1} KCl at 25 °C at a rate of 1.0 mL min^{-1}. Electronic spectra of MB solutions were recorded on a UV/VIS spectrophotometer (Unico 2100 Spectrophotometer, USA) at 663.8 nm. The concentration of MB was determined using a calibration curve made from standard MB solutions.

2.3 Methodology

2.3.1 Treatment of POR_{raw}

POR_{raw} was washed thoroughly with DW, dried at 80 °C to a constant mass, sieved to remove sand, manually cut with scissors, and sieved to a size lesser than 3.0 mm. The obtained material is named PPOR. Approximately 100 g of PPOR was soaked in 1 L of 1 mol L^{-1} acetic acid overnight, filtered, washed thoroughly with DW, dried at 80 °C for 24 h, and stored in polyethylene vials. This treated material was denoted "APOR."

2.3.2 Adsorption studies

The adsorption studies were performed at room temperature (23 ± 1.0 °C) and the ambient initial pH values of MB solutions of 4.8 unless otherwise stated. For the adsorption isotherm studies, batch experiments were conducted using 2.5 g $L^{-1}$of the adsorbent suspensions with initial concentrations ranging from 2 to 40 mg L^{-1} of MB (prepared by dissolving MB in deionized water) under shaking (180 r min^{-1}) for 10–90 min.

The amount of adsorbed MB (mg g^{-1}) at equilibrium (q_e) and at time t (q_t) was calculated from the mass balance expressions given by the following equations:

$$q_e = \frac{(C_0 - C_e)}{m} V \quad (1)$$

$$q_t = \frac{(C_0 - C_t)}{m} V \quad (2)$$

where C_0, C_e, and C_t are the liquid-phase concentrations (mg L^{-1}) of MB at the start, equilibrium, and time t, respectively. V (L) is the volume of solution and m (g) is the mass of adsorbent.

The thermodynamic studies of the adsorption of MB on APOR were performed at 23, 30, and 37 °C by adding 2.5 g L^{-1} of the adsorbent to a solution with an initial MB concentration of 40 mg L^{-1} and shaking for 10–60 min.

To investigate the effect of the initial pH on the adsorption behavior, 40 mg L^{-1} of MB was chosen as the initial concentration for an APOR dosage of 2.5 g L^{-1}. The initial pH (2.0–10) of MB solution was controlled using 0.1 M NaOH and HCl solutions. The resulting suspension containing adsorbent was then shaken for 60 min and the suspensions were centrifuged. The residual concentrations of adsorbate in the solution were finally determined.

2.3.3 Application

A batch experiment for the adsorption of MB from natural water samples spiked with 40 mg L^{-1} MB was performed. A dosage of 2.5 g L^{-1} was shaken in 20 mL of the water sample for 60 min at ambient pH and room temperature. Then, the samples were filtered and both the initial and residual (C_r) MB concentrations were determined. The removal efficiency (E_R%) was determined from the following formula:

$$E_R(\%) = \frac{C_0 - C_r}{C_0} x100 \quad (3)$$

Bivariate statistical correlations, which are a form of statistical analysis, used to find out if there is a relationship between two sets of values, were performed by using SPSS program.

3 Results and discussion

3.1 Characterization of PPOR and APOR

The chemical analysis of PPOR and its acetic acid-activated product APOR is shown in Table 1, which is compared with some reported analysis of PO rhizomes. The abundance of the studied elements in the PPOR was as follows: C > H > Ca > S > Mg > N > B > K > Fe > Sr > Al > Cu > Zn > Cr > Ba > Mn > Li > Co > Cd.

PPOR showed elemental contents within those reported for PO rhizomes except for C, Li, Ba, Cr, and Cu values, which were higher than those reported worldwide.

These high contents may be due to the nature of POR as offshore eco-waste. Some elemental contents in rhizomes were lower than those in leaves [3] such as N, H, Cr, and Fe, while some others were higher than those in leaves, such as C, S, Mg, Ba, Cu, and Zn. The distribution of metals in PO organs was reported previously to change depending on the site and time [30, 46]. This plant is valuable as a biomonitor for Cu, which is a necessary element for plant growth and metabolism [46]. The high level of pollution with heavy metals in the environment may be considered a reason for their high levels in rhizomes of PO. This conclusion was confirmed by the observation of metal contents of PPOR

Table 1 Elemental analysis (mg kg^{-1}) of PO rhizomes and APOR

Element	Present work		Reported values
	PPOR	APOR	PPOR
Li	4.85	3.56	0.58 (Sanz-LÃ¡zaro et al. [40])
K	1560.19	149.19	
Mg	7544.34	893.85	
Ca	19172.49	8348.54	
Sr	313.59	153.40	227 (Sanz-LÃ¡zaro et al. [40])
Ba	15.21	13.27	2.19 (Sanz-LÃ¡zaro et al. [40])
B	1924.27	122.01	
Al	259.87	166.02	19.28–52.42 [41]
Cr	35.60	12.30	2.35 [30], 0.24–1.27 [41], 16.56–36–81 [42], 5.93 (Sanz-LÃ¡zaro et al.[40])
Mn	9.39	3.88	4.22–9.61 [41], 9.1 (Sanz-LÃ¡zaro et al.[40])
Fe	372.49	354.05	48.49–370 [41], 411 (Sanz-LÃ¡zaro et al. [40])
Co	3.56	0.65	0.22–12.07 [41], 0.47 (Sanz-LÃ¡zaro et al. [40])
Cu	85.44	11.00	8.19 [30], 25.86–29.71 [43], 2.6–15.22 [41], 1.7–7.99 [42], 5.1 (Sanz-LÃ¡zaro et al. [40])
Zn	45.95	37.54	47.4 [30], 20–220 [41], 20.24–77.88 [42], 59 (Sanz-LÃ¡zaro et al. [40])
Cd	0.65	0.65	0.61 [30], 0.06–0.42 [43], 0.25–5.38 [41], 0.53 (Sanz-LÃ¡zaro et al. [40])
C (%)	44.72	47.36	32–38 [44]
N (%)	0.29	ND	1.0–2.5 [44], 0.8–1.3 [45]
H (%)	4.66	5.5	
S (%)	1.65	0.27	

within or close to those reported in Mediterranean Sea beaches. Despite the metal contents in PPOR samples were comparable to reported values, but APOR possessed obviously lower amounts of most of the analyzed elements in comparison with the untreated plant rhizome. The observed slight increase in the C and H contents of APOR relative to those of PPOR is in accordance with the anticipated relative increase in the percent hemicellulose and lignin that may be also due to the removal of inorganic deposits during acid activation process and the probable release of the metal-engaged acidic sites. These results are in accordance with the previously reported release of acidic sites accompanying the loss of metal contents [3].

The initial N and S contents in PPOR were remarkably reduced in APOR, which indicates the acid leaching of appreciable amounts of N and S.

The pH_{pzc} of APOR was observed at an appreciably lower value (2.0) compared with that of PPOR (7.72) as shown in Fig. 1. The observed reduction of pH_{pzc} of the acid-activated POR debris is an indication of the elimination of basic

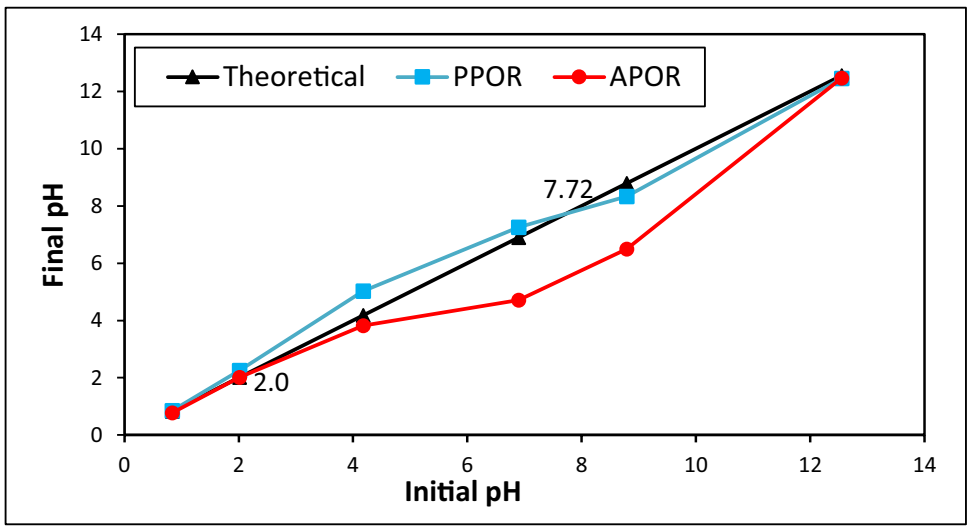

Fig. 1 pH_{pzc} of PPOR and APOR

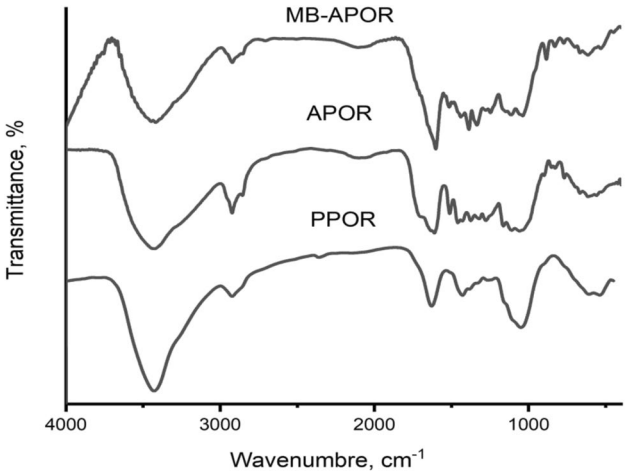

Fig. 2 FTIR spectra of PPOR, APOR and MB-APOR

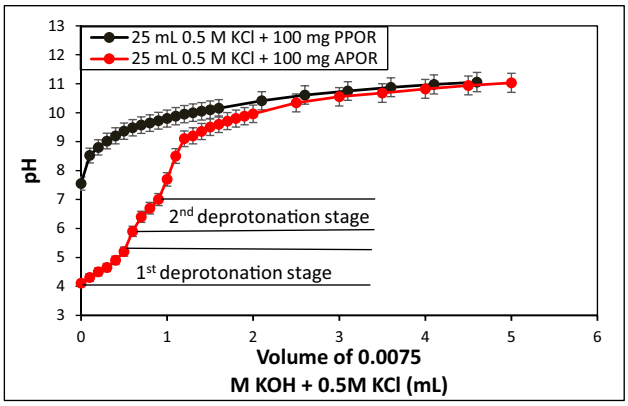

Fig. 3 pH-metric titration of PPOR and APOR

components such as calcium carbonate and the release of the cationic species occupying surface acidic sites, which fit with the observed metal content reduction in the above elemental analysis [3]. At the pH > pHzpc (pH 2), the surface of APOR became negatively charged due to deprotonation and hence enhancing electrostatic attraction with positively charged MB ions. FTIR (Fig. 2) confirmed this assumption from the disappearance of the IR absorption band observed at 1428 cm^{-1} assigned toν CO_3 in the FTIR absorption spectra of PPOR [3]. New shoulders were observed at 3340 and 1739 cm^{-1}, which are assignable to νOH and carbonyl νC = O vibrations respectively. The observation of a vibration for free COOH groups supports the possible release of the acidic sites bound to cationic species and/or the occurrence of a partial degradation. This is in accordance with the above-discussed measurements and the reported effect of acetic acid on plant fibers and cellulose [47].

The spectra of the MB-loaded APOR showed a blue shift in the wave number from 3426 cm^{-1} to 3433–3435 cm^{-1} and a red shift from 1636 cm^{-1} to 1629–1631 cm^{-1} which may indicate that the OH groups are involved in the adsorption of MB. This was also supported by the disappearance of the shoulders at 3340 and 1739 cm^{-1}. The shifting of peaks indicates that there was strong electrostatic interaction between adsorbate and adsorbent [48].

The pH-metric titration of PPOR and APOR against 0.0075 M KOH in 0.5 M KCl (Fig. 3) suggests the development of new acidic sites in APOR indicated by the appearance of two new deprotonation stages at pH 4.0–5.2 and 6.3–7.0 accounting for approximately 0.0657 mmol g^{-1} proton exchange capacity, which may be due to a partial hydrolysis of the ester groups, a release of the carboxylic groups engaged in ionic bonding, and a decomposition of the basic components, such as carbonates. This enhanced acidity was supported by an increase in the consumed volume of basic titrant by APOR compared with that consumed by PPOR between pH 4.5 and 8 and by the obvious shift in the pHpzc of APOR to the more acidic value of 2 compared with the value of 7.72 obtained for PPOR as shown in Fig. 1.

The nitrogen adsorption/desorption isotherms of PPOR and APOR (Fig. 4) correspond to type III according to the IUPAC classification [49]. The presence of type III adsorption isotherm is common with microporous materials that indicates an unrestricted multilayer formation process [49]. The textural properties of the two rhizome adsorbents are summarized in Table 2. S_{BET} values of PPOR and APOR were 46.61 and 23.71 m^2 g^{-1}; and average pore diameters values of PPOR and APOR were 1.44 and 4.26 nm, respectively. The widening of the average pore diameter of APOR upon activation of PPOR with acetic acid may be carried out by the removal of calcic deposits from PPOR pores.

The decrease in S_{BET} for APOR may be related to the removal of calcic and basic depositions on the dead PO rhizomes that may explain the unusual hysteresis for the desorption isotherm of PPOR [3]. The observed low surface area of the PO rhizomes is expected due to the compact structure of the rhizome as a supporting organ [50, 51]. However, it is reported that the adsorption capacity of activated carbon significantly depends on its pore diameter and pore volume [52]. The average pore diameter of the APOR in this study is 42°A (4.26 nm), and the reported size of MB dye molecule ranges from 5.91 to 13.82°A [52]. These findings suggest high capacity for MB adsorption due to the large size of APOR pores.

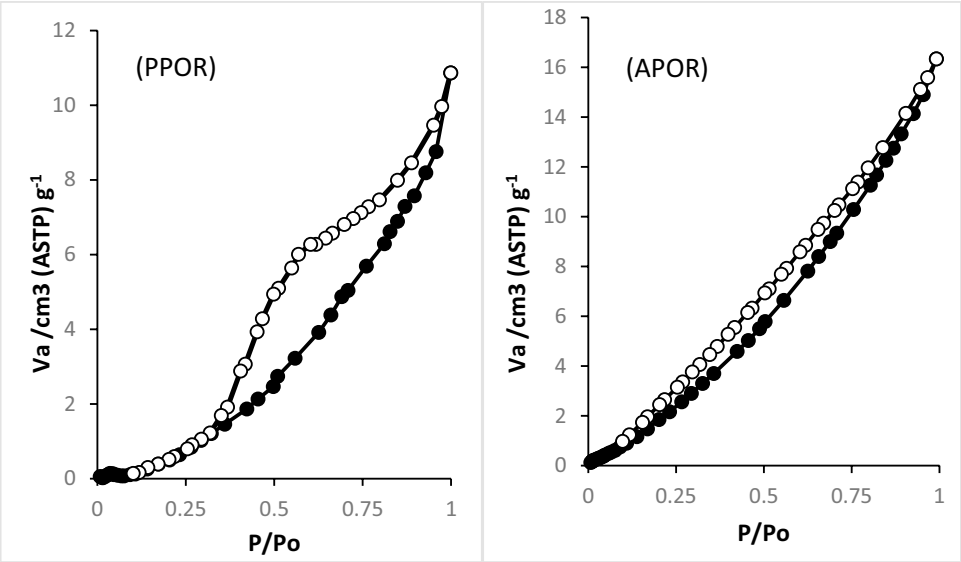

Fig. 4 Adsorption–desorption isotherm of N_2 on PPOR and APOR

Table 2 Textural properties of PPOR and APOR

Sample	BET ($m^2\ g^{-1}$)	Average pore diameter(nm)	Pore volume ($cm^3\ g^{-1}$)	C constant
PPOR	46.61	1.44	0.0168	0.172
APOR	23.71	4.26	0.0253	1.446

3.2 Adsorption studies

3.2.1 Effect of contact time and initial concentration of MB on the removal efficiency of PPOR and APOR

The effect of initial concentrations of MB (2.0–40.0 mg L^{-1}) on its removal efficiencies onto APOR and PPOR at the time of shaking 10–90 min is presented in Fig. 5.

APOR showed better removal efficiency compared to PPOR which is consistent with the above measurements, indicated by increased acidity, release of acidic groups, and the increase in the pore diameter and size. The time of shaking of 30 min was enough to approach equilibration, after which the removal efficiency slightly increased.

The kinetics of the adsorption process is regulated by characteristics of utilized adsorbate and adsorbent, as well as reaction steps involved in the whole process. To establish the kinetics of the MB adsorption in the present study, the time-dependent adsorption data was fitted to the mathematical relationship for pseudo-first-order model, pseudo-second-order model, and the intraparticle diffusion model which is based on liquid film mass transfer diffusion [53–55]. Kinetic studies performed indicated that the adsorption process of MB onto APOR follows the pseudo-2nd-order kinetic model

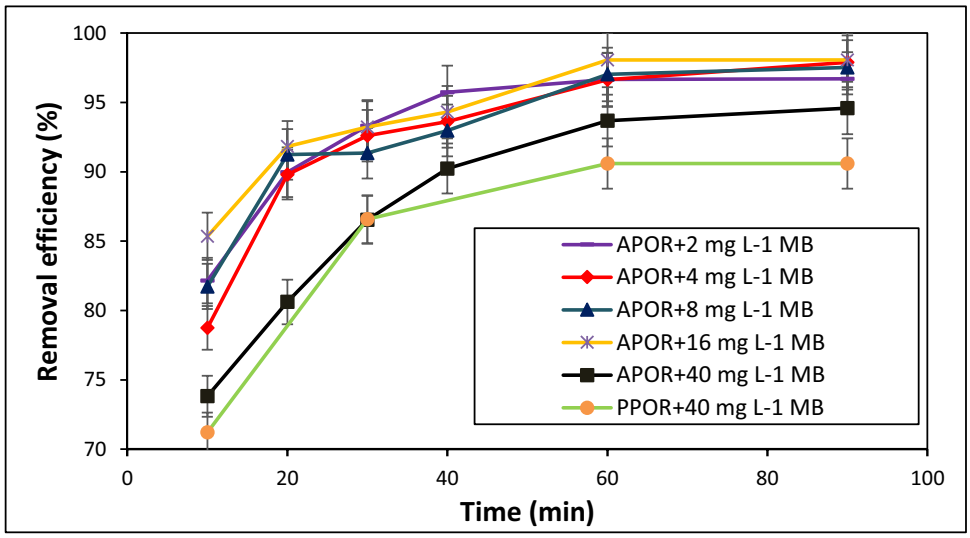

Fig. 5 The effect of shaking time on the removal efficiency (%) of MB with initial concentrations ranging from 2 to 40 mg L^{-1} on APOR and PPOR

where R^2 values are equal or very close to one and the calculated q_e values are mainly close to the q_e values from the experimental work; the obtained data are reported in Table 3. The results suggest that a heterogeneous adsorption mechanism is likely to be responsible for the uptake of MB onto APOR.

Table 3 Kinetic parameters for the adsorption models of MB onto APOR

Pseudo-first-order kinetic model				
C_0 (mg L^{-1})	q_e (mg g^{-1})		K_1 (min^{-1})	R^2
	Calculated	Experiment		
2.0	0.562	0.774	0.117	0.968
4.0	0.438	1.566	0.051	0.972
8.0	1.024	3.121	0.630	0.900
16	18.093	6.276	0.172	0.766
40	7.539	15.136	0.063	0.983
Pseudo-second-order kinetic model				
C_0 (mg L^{-1})	q_e (mg g^{-1})		K_2 (g $g^{-1}min^{-1}$)	R^2
	Calculated	Experiment		
2.0	0.792	0.774	0.691	1.000
4.0	1.613	1.566	0.228	0.999
8.0	3.205	3.121	0.129	1.000
16	6.423	6.276	0.078	1.000
40	15.848	15.136	0.016	0.999
Intraparticle diffusion rate kinetic model				
C_0 (mg L^{-1})	C (mg g^{-1})		K_p (mg g^{-1} $min^{-1/2}$)	R^2
2.0	0.6340		0.0172	0.7539
4.0	1.1999		0.0433	0.7958
8.0	2.4976		0.0729	0.8240
16	5.2275		0.1235	0.8644
40	10.5640		0.5376	0.8946

K_1, K_2, and K_p are the rate constant of the pseudo-1st-order and pseudo-2nd-order kinetic equations and the rate constant of the intraparticle diffusion model, respectively, while C is a constant related to the thickness of boundary layer

The adsorption isotherm of MB onto APOR fitting to Langmuir [56], Freundlich [57], Dubinin-Kaganer-Raduskavich (DKR) [58], Temkin [55, 59, 60], and Redlich and Peterson [61, 62] models was performed, and different isotherm equations are presented in Table 4.

Langmuir adsorption isotherm describes the homogeneous adsorbent surfaces where a monolayer of adsorbate is formed, and the maximum adsorption capacity (Qm, mg/g) corresponding to complete monolayer coverage on a surface of adsorbent can be estimated using the isotherm model. Freundlich isotherm describes the heterogeneous surface of adsorbents on which multilayer of adsorbate is formed and if the value of the constant n_F is higher than one, then it indicates that the adsorption of MB dye onto adsorbent is a favorable physical process [11, 24, 63], whereas the DKR isotherm model is attributed to the Polanyi potential theory, DKR evaluates the apparent free energy of porosity and the characteristic of adsorption. It assumes that the adsorption process continues until the pores are filled [55]. The mean free energy, derived from DKR model, provides information about whether the mechanism of adsorption is physical or chemical. The Temkin isotherm model considers the interaction between adsorbate and adsorbent. The Temkin model assumes that the adsorption heat of all molecules in the layer will decrease linearly with the accumulation of adsorbed molecules on the adsorbent surface [24, 64]. Redlich and Peterson (RP) suggested a three parameter adsorption isotherm model. The RP isotherm equation is mainly used to explain the formation of the monolayer with multisite interaction phenomena at the same time [65]. The three parameters of the Redlich–Peterson isotherm model are employed to study both homogeneous and heterogeneous adsorption systems [66]. Results are shown in Fig. 6 and Table 5.

Statistical error function analysis of isothermal models Error functions have been used by many researchers to select the appropriate isotherm model for adsorption. The error analysis of the isothermal models used in this study was performed

Table 4 Equations of the isotherm models used in this study

Isotherm model	Equation (linear form)	Equation no	Reference
Langmuir	$\frac{C_e}{q_e} = \frac{C_e}{q_{max}} + \frac{1}{K_L q_{max}}$	(4)	[56]
Freundlich	$\log q_e = \log K_F + {}^{1}/_{n} \log C_e$	(5)	[57]
Dubinin-Kaganer-Raduskavich (DKR)	$\ln q_e = \ln q_{max} - \frac{\varepsilon^2}{2E^2}$	(6)	[58]
Temkin	$q_e = \frac{RT}{b_T} \ln A_T + \frac{RT}{b_T} \ln C_e$	(7)	[60]
Redlich–Peterson (RP)	$\frac{C_e}{q_e} = \frac{1}{b_{RP} q'_{mon}} + \frac{1}{q'_{mon}} C_e^{\alpha}$	(8)	[62]

K_L, K_F, $1/n$, and E are the Langmuir and Freundlich adsorption constants, adsorption intensity, and mean adsorption energy respectively.ε (adsorption potential)$= RT\ln\left(\frac{1}{1+C_e}\right)$. b_T is Temkin constant which is correlated to the heat of sorption (J mol^{-1}) and A_T is Temkin isotherm constant (L g^{-1}). q'_{mon}, B_{RP}, and α are the R–P isotherm equation parameters. R is the general gas constant and T is the absolute temperature

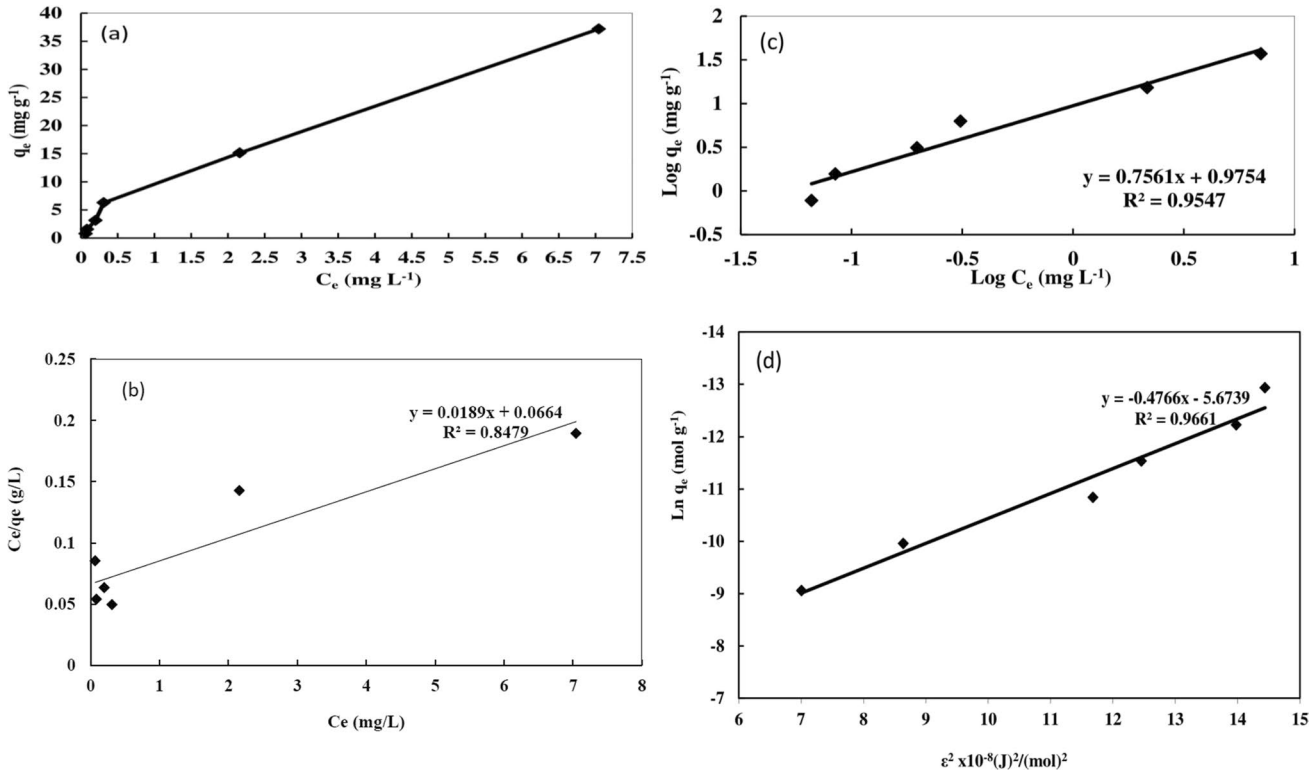

Fig. 6 Adsorption isotherm of MB onto APOR (**a**) and their linear fitting to Langmuir (**b**), Freundlich (**c**), DKR (**d**), Temkin (**e**), and Redlichand Peterson (**f**) adsorption models. ε (adsorption potential)= $RT\ln\left(\frac{1}{1+C_e}\right)$. R is the general gas constant and T is the absolute temperature

using the residual root mean squares (RMSE), sum square error (SSE), and chi-square test (X^2) functions where RMSE is the widely applied technique to foretelling the optimum isotherm at low concentrations [67], SSE is one the most utilized error functions, which provides a good match and the best value when we get close to zero [68], while the nonlinear chi-square (X^2 test is useful to show if the experimental result matched the expected data; the X^2 is a parametric test based on the distribution of the difference from normal distribution, small values of chi-square test refer their resemblance, while a larger numbers refer to the difference of the empirical result [69]. Error function equations are listed in Table 6 and results are shown in Table 7.

According to the used error function analysis, the best fit isotherm model with the lowest error function results is the Temkin isotherm model. The smaller the error function values indicate similarity between the experimental data of MB adsorption on APOR and the values calculated using the theoretical isotherm. Temkin isotherm model considers that the heat of adsorption of all molecules in the layer will decrease over time with the accumulation of adsorbed molecules on the adsorbent surface [24]. The isotherm model takes into account the interaction between adsorbate and adsorbent. Temkin linear equation is presented in Table 4 and Eq. (7), where A_T is the equilibrium binding constant corresponding to the maximum binding energy and constant β, which is equal to RT/b_T (J mol^{-1}), indicates the heat of sorption, b_T is employed to determine the type of adsorption process, R is the universal gas constant (8.314 J K^{-1} mol^{-1}), and T is the absolute temperature in Kelvin. All of these parameters were determined from the plot between q_e and lnC_e. If the value of β parameter is less than 8 kJ/mol, this indicates a weak interaction between MB and the surface of APOR [70]. If b_T value is <80, this means that the adsorption process is of physical nature [70]. The values from Temkin isotherm were $b_T = 1.13 \times 10^8$, then the adsorption of the first layer is mainly not physical adsorption and the value of β is less than 8 kJ/mol, indicating a weak interaction between MB and the surface of APOR, which may be attributed to minor physical adsorption in the first layer. The values of b_T and A_T which is corresponding to the binding energy indicate that the first layer is predominated by chemical adsorption [55, 71].

Considering the correlation coefficients, R^2 values of the different isotherm models, it was observed that a good fitness of the studied adsorption models for MB on APOR is found with the DKR and Freundlich isotherm models (Table 4, Eqs. (6) and (5) respectively). The DKR was the most matching model with a linear regression coefficient

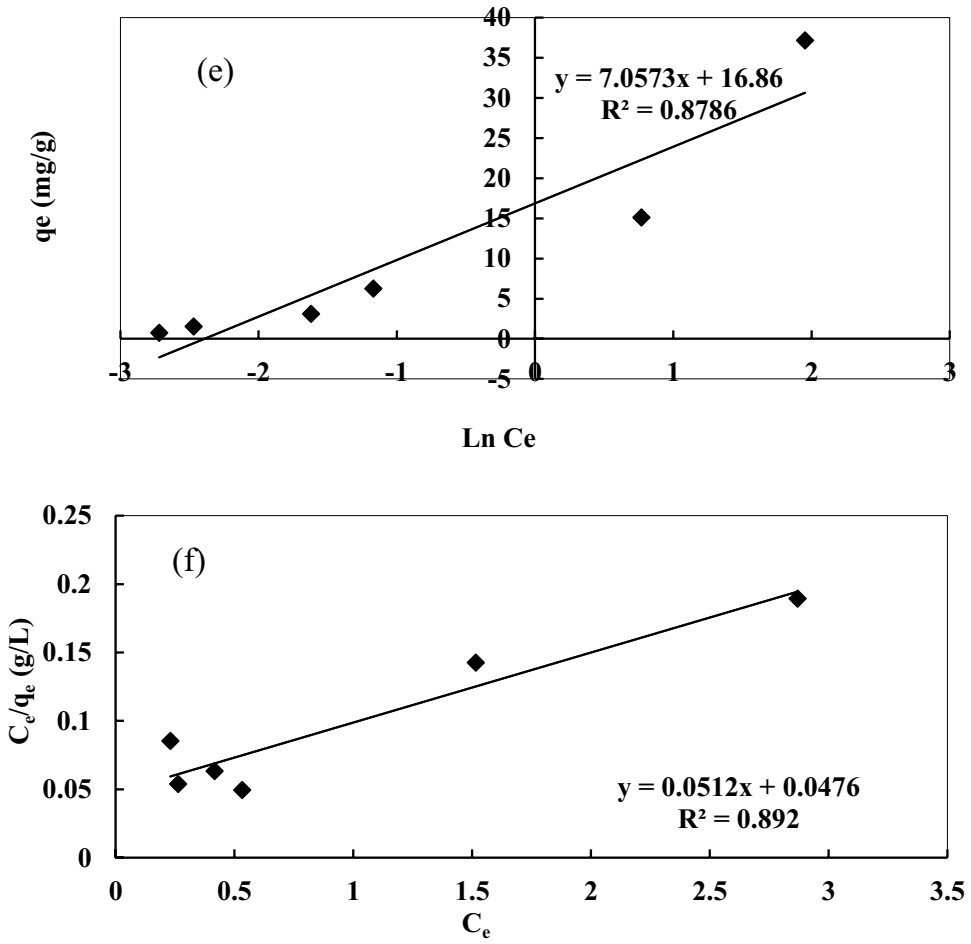

Fig. 6 (continued)

Table 5 Isotherm model parameters for the adsorption of MB onto APOR

Langmuir isotherm parameters				
q_{max} (mg g^{-1})		K_L	R_L	R^2
52.91		0.285	0.034–0.637	0.848
Freundlich isotherm parameters				
1/*n*		K_F (mg/g)		R^2
0.756		9.449		0.955
DKR isotherm parameters				
q_{max} (mg g^{-1})		*E* (kJ/mol)		R^2
1097		10.242		0.966
Temkin isotherm parameters				
b_T	$\beta = RT/\ b_T$ (J mol^{-1})	A_T (L/mg)		R^2
1.13×10^8	2.21×10^{-5}	3.487×10^6		0.8786
Redlich–Peterson isotherm parameters				
q'_{mon} (mg g^{-1})	b_{RP} (L^3 g^{-1})	α		R^2
19.531	1.076	0.54		0.892

K_L and K_F are the Langmuir and Freundlich adsorption constants; 1/*n* adsorption intensity, *E* mean adsorption energy, b_T, and A_T are the Temkin isotherm constants; and q'_{mon}, b_{RP}, and α are the Redlich–Peterson isotherm equation parameters

Table 6 Error function equations

Model name	Equation Formula	Best fit	Equation number
SSE	$\sum_{i=1}^{n}(q_{ecal}-q_{eexp})_i^2$	Smallest value	(9)
RMSE	$100\sqrt{\frac{1}{N}\sum_{i=1}^{N}(1-\frac{q_{eexp}}{q_{ecal}})^2}$	Smallest value	(10)
Chi-square	$\sum_{i=1}^{n}\frac{(q_{eexp}-q_{ecal})_i^2}{q_{ecal}}$	Smallest value	(11)

Table 7 Statistical error function analysis of different isothermal models

Isotherm model	RMSE	SSE	X^2
Langmuir	0.0024	0.0160	2.77E − 02
Freundlich	0.0884	1.9525	5.43E − 01
Dubinin-Radushkevich	0.3513	10.3520	3.02E − 02
Temkin	1.163E − 9	9.579E − 9	5.44E − 05
Redlich–Peterson	0.0017	0.016	2.38E − 02

(R^2) closest to one and maximum adsorption capacity q_{max} (1097 mg g^{-1}) for MB adsorption on APOR. The high value of q_m is expected due to the significant increase in the pore size and diameter of APOR during the activation process and the DKR model assumes that the adsorption process continues until the pores are filled [55]. The positive value of adsorption energy $E = 10.242$ kJ mol^{-1} obtained for MB indicates that the adsorbate is chemically adsorbed onto APOR in endothermic processes. The obtained adsorption capacity of APOR towards MB is remarkably higher than many adsorbents such as chitosan/zeolite composite (24.5 mg g^{-1} [72]) activated carbon obtained from *Posidonia oceanica* dead leaves (285.7 mg g^{-1} [36]) or acrylic waste (8.76 mg g^{-1} [73]), citrus limetta peel waste (227.3 mg g^{-1} [74]), and Marine green algae *Ulva lactuca* (344.83 mg g^{-1} [24]). The value of Freundlich isotherm constant, n_F, is higher than one, which may indicate that the adsorption of MB dye onto APOR is a multilayer favorable physical process. The chemical adsorption suggested by the DKR and Temkin isotherm models is supported by the electrostatic interactions between the functional groups (-CO and $-COO^-$) available on the APOR surface and MB^+ ions in solution (-CO-MB and -C-OO-MB) as suggested by FTIR spectrum given in Fig. 2. Hence, suggested combined electrostatic and physical adsorptions may be responsible for the removal of MB from water by APOR where chemisorption predominates the first layer followed by physisorption on the subsequent layers through adsorbate–adsorbate interaction.

3.2.2 Effect of temperature

The effect of temperature (23–37 °C) on the adsorption of MB onto APOR is shown in Fig. 7, and adsorption was observed to increase with increasing the temperature, which is consistent with the DKR results. The increase in adsorption with increasing the temperature may be attributed to increasing the kinetic energy of the molecules and in turn increasing the diffusion of MB and hence the chances of collision between APOR and MB ions. This is in agreement with the results from DKR isotherm supporting the endothermic nature of the process.

The observed preferred warm conditions for the adsorption process are very optimal for the application in the Mediterranean Sea weather.

3.2.3 Effect of initial solution pH

The effect of initial pH of the solution on the adsorption of MB onto APOR is studied. The experiment was performed at a pH ranging from 2 to 10, results are shown in Fig. 8, and adsorption was found to increase with increasing pH with maximum removal efficiency at pH 8.0. The MB dye gives positive ions when dissolved in water. Then, in an acidic pH, the positively charged absorbent surface tends to counteract the absorption of the cationic dye. The increase in pH of the solution made the surface of adsorbent become negatively charged, which resulted in increased adsorption of the MB dye as a result of increased electrostatic attraction force that occurred between the negatively charged surface of APOR and the positively charged MB dye [24]. These conditions are optimal for natural water.

3.3 Application

The removal efficiency of MB by APOR was examined on natural water samples spiked with 40 mg L^{-1} MB, and adsorbent dosage of 2.5 g L^{-1} was shaken in 20 mL of the

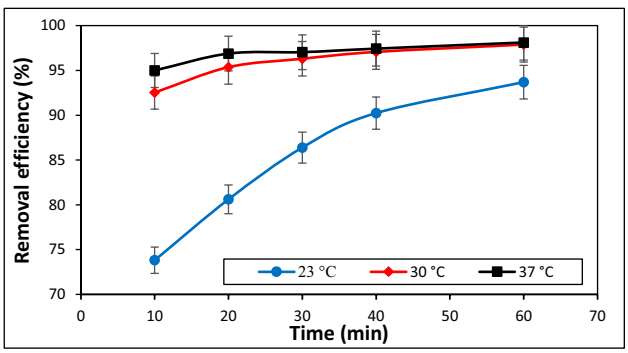

Fig. 7 Effect of temperature on the adsorption efficiency of MB (40 mg L^{-1}) on APOR (2.5 g L^{-1})

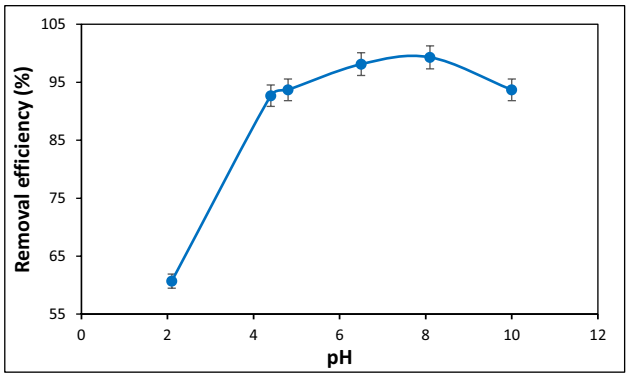

Fig. 8 Effect of initial pH of the solution on the percent removal efficiency of MB on APOR

water sample for 60 min at ambient pH and room temperature. Natural water samples were collected from different sites along the coasts of Gamassa, Port Said, Hurghada, Burullus, and Manzala lakes as detailed in Table 8. The water samples are characterized by quite versatile salinities ranged from seawater samples (TDS, g L^{-1}, 26.00–40.18) to brackish water from Burullus and Manzala lakes (TDS, g L^{-1}, 0.90–21.63). The low salinity values in some seawater samples are due to domestic inflows of freshwaters while the saline origin of the lake waters overflows the Mediterranean Sea water through water exchange canals. The initial pH values of the water samples ranged from 7.25 for freshwater-influenced sites to 8.55 for seawaters, which are within the recommended range for high adsorption of MB onto APOR. The final pH values after the adsorption process slightly dropped within 0–1.15.

The removal efficiencies ranged from 51.7 at Bahr Kromlos, Manzala Lake, in winter to 97.2% at the 15th May coast, Gamassa. The bivariate statistic evaluation of results revealed that E_R% values were not influenced by the initial pH values (Pearson Correlation = 0.246), which is in agreement with the pH study. Moreover, a significant positive correlation between the removal efficiency and TDS is found (Pearson correlation = 0.585), which indicates that despite the high cationic competition in saline water, APOR is appropriate for its water applications due to its oceanographic origin. The difference between the high q_{max} of DKR and the obtained values is possibly due to the adsorption of a monolayer of MB molecules on the surface of the APOR, which is also supported by Temkin isotherm results, forming an outside coverage which causes resistance for deeper MB diffusion [52], and the monolayer is then followed by multi-layer physical adsorption formation [3].

Table 8 Removal efficiency (E_R%) of APOR for MB-spiked water samples from Gamassa, Port Said, and Hurghada coastal waters. C_i = 40 mg L^{-1} MB, dosage 2.5 g L^{-1} of APOR, and time of stirring = 60 min

Sample			TDS g L^{-1}	$pH_{(i)}$	$pH_{(f)}$	E_R%
Manzala Lake	Winter	Elzarka	7.50	7.78	7.19	88.9
		Bahr Kromlos	2.20	7.9	7.27	51.7
		Deshdy	4.00	7.94	7.32	80.6
		Genka	2.00	7.73	7.7	67.3
		Elbashtir	3.40	7.87	7.66	68.0
		Temsah	20.00	7.25	7.25	85.3
	Summer	Elzarka	1.00	7.71	7.65	76.4
		Bahr Kromlos	1.20	7.83	7.32	78.8
		Deshdy	0.90	7.42	7.16	75.2
		Genka	1.00	7.81	7.53	74.2
		Elbashtir	1.20	7.86	7.64	78.5
		Temsah	4.50	7.72	7.63	68.3
Port Said	Elborg Rest		26.00	8.02	7.00	93.0
	Army Hotel		32.29	8.02	7.15	84.9
Gamassa	Ellesan		26.71	8.04	7.15	78.5
	Amon		40.18	7.29	7.17	84.2
	15th May		40.18	7.60	7.10	97.2
Hurgada			30.00	8.30	7.15	95.6
Burullus Lake	Tera		4.24	8.20	-	91.3
	Bughaz		21.63	8.17	-	87.9
	East		6.15	8.55	-	90.5

4 Conclusions

The debris of *Posidonia oceanica rhizomes* (POR) were effectively activated via a simple and fast acetic acid treatment which led to an elimination of basic components and release of cationic species occupying surface acidic sites, in addition to development of new acidic sites. Kinetic studies performed indicated that the adsorption process of MB onto APOR followed pseudo-2nd-order kinetic model. Application of different error functions revealed that Temkin isotherm is the most appropriate model with a b_T value of 1.13×10^8, β value less than 8 kJ/mol, and high A_T value of 3.487×10^6, which indicates a chemically adsorbed monolayer. While based on the linear regression coefficient (R^2), DKR was the most matching model with (R^2) value of 0.966 and maximum adsorption capacity q_{max} (1097 mg g^{-1}) for MB adsorption on APOR, with a positive value of adsorption energy $E = 10.242$ kJ mol^{-1} which indicates that the adsorbate is chemically adsorbed onto APOR in endothermic processes. The DKR was followed by Freundlich isotherm model with (n) value higher than one, indicating a multilayer favorable physical adsorption. A suggested, endothermic, multilayer, combined electrostatic and physical adsorption mechanism may be responsible for the removal of MB from water by APOR. Adsorption is expected to begin with chemisorption on active surface functional groups of adsorbent's surface followed by physisorption on the subsequent layers through adsorbate–adsorbate interaction.

Adsorption of MB onto APOR was observed to increase with increasing temperature within the studied range (23–37 °C) and within a wide pH range from 4 to 10 with a maximum value at pH 8.0. The time of shaking of 30 min was enough to reach equilibration. The removal efficiency of MB by APOR was examined on spiked water samples from different sites along the northeast coasts. A maximum removal efficiency of > 97% was achieved, which indicates that despite the high cationic competition in saline water, APOR is appropriate for applications due to its oceanographic origin. In conclusion, *Posidonia oceanica rhizomes* which is currently imposing an environmental risk can be effectively used, after acid activation, as a cost-effective adsorbent for the removal of MB as a model cationic dye from polluted brackish and saline waters with high efficiency.

Supplementary Information The online version contains supplementary material available at https://doi.org/10.1007/s13399-022-02709-5.

Acknowledgements The authors wish to thank Prof. Seham Shaban, Egyptian Petroleum Research Institute, Cairo, Egypt, for cooperation and Dr. Asmaa Ahmed El-Halag, from the Faculty of Engineering, Delta University, for her assistance during the preparation of this manuscript.

Author contribution Khaled S. Abou-El-Sherbini and Randa R. Elmorsi suggested the idea of the paper and collected the seagrass debris and water samples; Hesham R. Lotfy and Khaled S. Abou-El-Sherbini conceived the experiments; Randa R. Elmorsi, Waleed A. Shehab El-Dein and Khaled S. Abou-El-Sherbini conducted the experiments; and Hesham R. Lotfy and Khaled S. Abou-El-Sherbini analyzed the results. All authors reviewed the manuscript.

Funding Open access funding provided by The Science, Technology & Innovation Funding Authority (STDF) in cooperation with The Egyptian Knowledge Bank (EKB).

Declarations

Conflict of interest The authors declare no competing interests.

References

1. Mia R, Selim M, Shamim AM et al (2019) Review on various types of pollution problem in textile dyeing & printing industries of Bangladesh and recommandation for mitigation. J Text Eng Fash Technol 5:220–226. https://doi.org/10.15406/jteft.2019.05.00205
2. Berradi M, Hsissou R, Khudhair M et al (2019) Textile finishing dyes and their impact on aquatic environs. Heliyon 5:. https://doi.org/10.1016/j.heliyon.2019.e02711
3. Elmorsi RR, El-Wakeel ST, Shehab El-Dein WA et al (2019) Adsorption of Methylene Blue and Pb^{2+} by using acid-activated Posidonia oceanica waste. Sci Rep 9:3356. https://doi.org/10.1038/s41598-019-39945-1
4. Vilardi G, Bubbico R, Palma L. D, Verdone N (2020) Nitrate green removal by fixed-bed columns packed with waste biomass: modelling and friction parameter estimation. Chem Eng Res Des 154: 250-261, ISSN 0263-8762, https://doi.org/10.1016/j.cherd.2019.12.020
5. Zafar MS, Ahmad SW, Mubeen A, Khan WA (2018) Removal of residual carcinogenic dyes from industrial wastewater. Chem Ind Chem Eng 24:69–76
6. Abou-El-Sherbini KS, Kenawy IMM, Hafez MAH, et al (2015) Synthesis of novel CO_3^{2-}/Cl^--bearing 3(Mg + Zn)/(Al + Fe) layered double hydroxides for the removal of anionic hazards. J Environ Chem Eng 3:. https://doi.org/10.1016/j.jece.2015.09.015
7. Joseph NT, Chigozie UF (2014) Effective decolorization of eriochrome black T, furschin basic and malachite green dyes from synthetic wastewater by. Chem Process Eng Res 21:98–107
8. Karimi M, Mohsen-Nia M, Akbari A (2014) Electro-separation of synthetic azo dyes from a simulated wastewater using polypyrrole/

polyacrylonitrile conductive membranes. J Water Process Eng 4:6–11. https://doi.org/10.1016/j.jwpe.2014.08.008
9. Ngulube T, Gumbo JR, Masindi V, Maity A (2017) An update on synthetic dyes adsorption onto clay based minerals: a state-of-art review. J Environ Manage
10. Soares PA, Batalha M, Souza SMAGU et al (2015) Enhancement of a solar photo-Fenton reaction with ferric-organic ligands for the treatment of acrylic-textile dyeing wastewater. J Environ Manage 152:120–131. https://doi.org/10.1016/j.jenvman.2015.01.032
11. Siddiqui SI, Chaudhry SA (2019) Nanohybrid composite Fe_2O_3-ZrO_2/BC for inhibiting the growth of bacteria and adsorptive removal of arsenic and dyes from water. J Clean Prod. 223: 849-868, ISSN 0959-6526, https://doi.org/10.1016/j.jclepro.2019.03.161
12. Choudhry A, Sharma A, Alam Khan T, Chaudhry SA (2021) Flax seeds based magnetic hybrid nanocomposite: an advance and sustainable material for water cleansing. J Water Process Eng 42: 102150 ISSN 2214-7144, https://doi.org/10.1016/j.jwpe.2021.102150
13. Fatima B, Siddiqui SI, Nirala RK, Vikrant K, Kim KH, Ahmad R, Chaudhry S A (2021) Facile green synthesis of ZnO–$CdWO_4$ nanoparticles and their potential as adsorbents to remove organic dye. Environ Pollut 271: 116401, ISSN 0269-7491, https://doi.org/10.1016/j.envpol.2020.116401
14. Chinh VD, Bavasso I, Di Palma L (2021) Enhancing the photocatalytic activity of TiO_2 and TiO_2–SiO_2 by coupling with graphene–gold nanocomposites. J Mater Sci: Mater Electron 32:5082–5093. https://doi.org/10.1007/s10854-021-05242-9
15. Rafique M, Hajra S, Tahir MB et al (2022) A review on sources of heavy metals, their toxicity and removal technique using physico-chemical processes from wastewater. Environ Sci Pollut Res. https://doi.org/10.1007/s11356-022-18638-9
16. Chinh VD, Hung LX, Di Palma L, Hanh VTH, Vilardi G (2019) Effect of carbon nanotubes and carbon nanotubes/gold nanoparticles composite on the photocatalytic activity of TiO_2 and TiO_2-SiO_2. Chem Eng Technol 42:308–315. https://doi.org/10.1002/ceat.201800265
17. Lellis B, Fávaro-Polonio CZ, Pamphile JA, Polonio JC (2019) Effects of textile dyes on health and the environment and bioremediation potential of living organisms. Biotechnol Res Innov 3:275–290. https://doi.org/10.1016/j.biori.2019.09.001
18. Talaiekhozani A, Rezania S (2017) Application of photosynthetic bacteria for removal of heavy metals, macro-pollutants and dye from wastewater: a review. J Water Process Eng 19:312–321. https://doi.org/10.1016/j.jwpe.2017.09.004
19. Watharkar AD, Khandare RV, Waghmare PR et al (2015) Treatment of textile effluent in a developed phytoreactor with immobilized bacterial augmentation and subsequent toxicity studies on Etheostoma olmstedi fish. J Hazard Mater 283:698–704. https://doi.org/10.1016/j.jhazmat.2014.10.019
20. Abdulla NK, Siddiqui SI, Fatima B, Sultana R, Tara N, Hashmi AA, Ahmad R, Mohsin M, Nirala RK, Linh NT, Bach Q-V, Chaudhry SA (2021) Silver based hybrid nanocomposite: a novel antibacterial material for water cleansing. J Clean Prod 284:124746. https://doi.org/10.1016/j.jclepro.2020.124746
21. Hafez MAH, Kenawy IMM, Abd Elbary ZME et al (2019) Removal of Cr(VI) from aqueous media on calcined (Mg-Zn)/(Al-Fe)-(CO_3)/Cl layered double hydroxides. Desalin Water Treat 148:270–284. https://doi.org/10.5004/dwt.2019.23742
22. Abdolali A, Guo WS, Ngo HH et al (2014) Typical lignocellulosic wastes and by-products for biosorption process in water and wastewater treatment: a critical review. Bioresour Technol 160:57–66. https://doi.org/10.1016/j.biortech.2013.12.037
23. Ben-Ali S, Jaouali I, Souissi-Najar S, Ouederni A (2017) Characterization and adsorption capacity of raw pomegranate peel biosorbent for copper removal. J Clean Prod 142:3809–3821. https://doi.org/10.1016/j.jclepro.2016.10.081
24. El Nemr A, Shoaib AGM, El Sikaily A et al (2021) Evaluation of cationic methylene blue dye removal by high surface area mesoporous activated carbon derived from *Ulva lactuca*. Environ Process 8:311–332. https://doi.org/10.1007/s40710-020-00487-8
25. Noor NM, Othman R, Mubarak NM, Abdullah EC (2017) Agricultural biomass-derived magnetic adsorbents: preparation and application for heavy metals removal. J Taiwan Inst Chem Eng 78:168–177. https://doi.org/10.1016/j.jtice.2017.05.023
26. Wanyonyi WC, Onyari JM, Shiundu PM (2014) Adsorption of congo red dye from aqueous solutions using roots of eichhornia crassipes: kinetic and equilibrium studies. Energy Procedia 50:862–869. https://doi.org/10.1016/j.egypro.2014.06.105
27. Elmorsi RR, Mostafa GAH, Abou-El-Sherbini KS (2021) Homoionic soda-activated bentonite for batch-mode removal of Pb(II) from polluted brackish water. J Environ Chem Eng 9:104606. https://doi.org/10.1016/j.jece.2020.104606
28. Ontoria Y, Gonzalez-Guedes E, Sanmartí N et al (2019) Interactive effects of global warming and eutrophication on a fast-growing Mediterranean seagrass. Mar Environ Res 145:27–38. https://doi.org/10.1016/j.marenvres.2019.02.002
29. Ruiz JM, Marín-Guirao L, García-Muñoz R, et al (2017) Experimental evidence of warming-induced flowering in the Mediterranean seagrass Posidonia oceanica. Mar Pollut Bull 0–1. https://doi.org/10.1016/j.marpolbul.2017.10.037
30. Bonanno G, Di Martino V (2017) Trace element compartmentation in the seagrass Posidonia oceanica and biomonitoring applications. Mar Pollut Bull 116:196–203. https://doi.org/10.1016/j.marpolbul.2016.12.081
31. Copat C, Maggiore R, Arena G et al (2012) Evaluation of a temporal trend heavy metals contamination in Posidonia oceanica (L.) Delile, (1813) along the western coastline of Sicily (Italy). J Environ Monit 14:187–192. https://doi.org/10.1039/c1em10575b
32. Hernández-Martínez AM, Padrón-Sanz C (2013) Determination of Ni, Cr, Cu, Pb and Cd on the Mediterranean endemic plant Posidonia oceanica using the green extraction method "Microwave Assisted Micellar Extraction" and GFAAS. Anal Methods 5:6473. https://doi.org/10.1039/c3ay41310a
33. Lafabrie C, Pergent G, Kantin R et al (2007) Trace metals assessment in water, sediment, mussel and seagrass species - validation of the use of Posidonia oceanica as a metal biomonitor. Chemosphere 68:2033–2039. https://doi.org/10.1016/j.chemosphere.2007.02.039
34. Coletti A, Valerio A, Vismara E (2013) Posidonia oceanica as a renewable lignocellulosic biomass for the synthesis of cellulose acetate and glycidyl methacrylate grafted cellulose. Materials (Basel) 6:2043–2058. https://doi.org/10.3390/ma6052043
35. Cavas L, Karabay Z, Alyuruk H et al (2011) Thomas and artificial neural network models for the fixed-bed adsorption of methylene blue by a beach waste Posidonia oceanica (L.) dead leaves. Chem Eng J 171:557–562. https://doi.org/10.1016/j.cej.2011.04.030
36. Dural MU, Cavas L, Papageorgiou SK, Katsaros FK (2011) Methylene blue adsorption on activated carbon prepared from Posidonia oceanica (L.) dead leaves: kinetics and equilibrium studies. Chem Eng J 168:77–85. https://doi.org/10.1016/j.cej.2010.12.038
37. Chadlia A, Mohamed K, Najah L, Farouk MM (2009) Preparation and characterization of new succinic anhydride grafted Posidonia for the removal of organic and inorganic pollutants. J Hazard Mater 172:1579–1590. https://doi.org/10.1016/j.jhazmat.2009.08.030
38. Dridi-Dhaouadi S, Douissa-Lazreg NB, M' Henni MF (2011) Removal of lead and Yellow 44 acid dye in single and binary component systems by raw Posidonia oceanica and the cellulose extracted from the raw biomass. Environ Technol 32:325–340. https://doi.org/10.1080/09593330.2010.499545

39. Lefebvre L, Compère P, Léonard A et al (2021) Mediterranean aegagropiles from Posidonia oceanica (L.) Delile (1813): a first complete description from macroscopic to microscopic structure. Mar Biol 168:1–17. https://doi.org/10.1007/s00227-021-03833-y
40. Sanz-LÃ¡zaro C, Malea P, Apostolaki ET et al (2012) The role of the seagrass Posidonia oceanica in the cycling of trace elements. Biogeosci Discuss 9(2623):2653. https://doi.org/10.5194/bgd-9-2623-2012
41. Tovar-Sánchez A, Serón J, Marbà N, et al (2010) Long-term records of trace metal content of western Mediterranean seagrass (Posidonia oceanica) meadows: Natural and anthropogenic contributions. J Geophys Res G Biogeosci 115:. https://doi.org/10.1029/2009JG001076
42. Saliha B-T, Waffa H, Mourad B (2016) Assessment of metallic trace elements using the seagrass Posidonia oceanica and the surface sediment from north eastern of Algeria. Asian J Biol Sci 10:17–26. https://doi.org/10.3923/ajbs.2017.17.26
43. Cozza R, Iaquinta A, Cozza D, Ruffolo L (2013) Trace metals in Posidonia oceanica in a coastal area of the Ionian Sea (Calabria, Italy). Open J Ecol 03:102–108. https://doi.org/10.4236/oje.2013.32012
44. Balestri E, Gobert S, Lepoint G, Lardicci C (2009) Seed nutrient content and nutritional status of Posidonia oceanica seedlings in the northwestern Mediterranean Sea. Mar Ecol Prog Ser 388:99–109. https://doi.org/10.3354/meps08104
45. Lepoint G, Vangeluwe D, Eisinger M et al (2004) Nitrogen dynamics in Posidonia oceanica cuttings: implications for transplantation experiments. Mar Pollut Bull 48:465–470. https://doi.org/10.1016/j.marpolbul.2003.08.023
46. Gosselin M, Bouquegneau JM, Lefèbvre F et al (2006) Trace metal concentrations in Posidonia oceanica of North Corsica (northwestern Mediterranean Sea): use as a biological monitor? BMC Ecol 6:1–19. https://doi.org/10.1186/1472-6785-6-12
47. Dupont A-L, Tétreault J, Tetreault J (2000) Cellulose degradation in an acetic acid environment. Stud Conserv 45:201
48. Thabede PM, Shooto ND, NaidooE B (2020) Removal of methylene blue dye and lead ions from aqueous solution using activated carbon from black cumin seeds. S Afr J Chem Eng 33:39–50. https://doi.org/10.1016/j.sajce.2020.04.002
49. Sing KSW (1982) Reporting physisorption data for gas/solid system with special reference to the determination of surface area and porosity. Pure App Chem 54:2201–2218
50. Jung J, Lee SC, Choi HK (2008) Anatomical patterns of aerenchyma in aquatic and wetland plants. J Plant Biol 51:428–439. https://doi.org/10.1007/BF03036065
51. Haznedarolu MZ, Akarsu F (2009) Anatomical features of Posidonia oceanica (L.) Delile growing in Turkey. Hacettepe Univ J Fac Pharm 29:37–43
52. Nguyen HT, Khang D, Hai T, Dinh N, PhanDinh T (2021) Methylene blue adsorption mechanism of activated carbon synthesised from cashew nut shells. RSC Adv 11:26563–26570. https://doi.org/10.1039/d1ra04672a
53. Srinivasan K, Balasubramanian N, Ramakrishan TV (1988) Studies on chromium removal by rice husk carbon. Indian J Environ Health 30:376–387
54. Weber WJ, Morris JC (1963) Kinetics of adsorption on carbon from solution. J Sanit Eng Div Am Soc Civil Eng 89:31–60
55. El-Nemr M, Yılmaz M, Ragab S, El Nemr A (2022) Biochar-SO prepared from pea peels by dehydration with sulfuric acid improves the adsorption of Cr^{6+} from water. Biomass Conversion and Biorefinery. https://doi.org/10.1007/s13399-022-02378-4
56. Langmuir I (1918) The adsorption of gases on plane surfaces of glass, mica and platinum. J Am Chem Soc 40:1361–1403. https://doi.org/10.1021/ja02242a004
57. Freundlich HMF (1906) Uber die adsorption in losungen, Z. Phys Chem 57A:385–470
58. Cortes J, Araya P (1986) The Dubinin-Radushkevich-Kaganer equation. J Chem SOC Furaday Trans I. https://doi.org/10.1039/F19868202473
59. Kavitha D, Namasivayam C (2007) Experimental and kinetic studies on methylene blue adsorption by coirpith carbon. Bioresour Technol 98:14–21
60. Tempkin MJ, Pyzhev V (1940) Kinetics of ammonia synthesis on promoted iron catalysts. Acta Physiochimica URSS 12:217–222
61. Aloui, Amel & Bouziane, Nouzha & Bendjeffal, Hacene & Bouhedja, Yacine & Zertal, Abdennour (2021) Biosorption of some pharmaceutical compounds from aqueous medium by Luffa cylindrica fibers: application of the linear form of the Redlich-Peterson isotherm equation. Desalin Water Treat 214. https://doi.org/10.5004/dwt.2021.26736
62. Wu F-C, Liu B-L, Wu K-T, Tseng R-L (2010) A new linear form analysis of Redlich-Peterson isotherm equation for the adsorptions of dyes. Chem Eng J 162:21–27. https://doi.org/10.1016/j.cej.2010.03.006
63. khalatbary M, Sayadi M, Hajiani M, Nowrouzi M (2022) Adsorption studies on the removal of malachite green by γ-Fe2O3/MWCNTs/cellulose as an eco-friendly nanoadsorbent. Biomass Conversion and Biorefinery. 1-19. https://doi.org/10.1007/s13399-022-02475-4
64. Foo KY, Hameed BH (2010) Insights into the modeling of adsorption isotherm systems. Chem Eng J 156(1):2–10. https://doi.org/10.1016/j.cej.2009.09.013
65. Redlich O, Peterson DL (1959) A useful adsorption isotherm. J Phys Chem 63:1024
66. Vilela PB, Dalalibera A, Duminelli EC, Becegato VA, Paulino AT (2019) Adsorption and removal of chromium (VI) contained in aqueous solutions using a chitosan-based hydrogel. Environ Sci Pollut Res 26:28481–28489
67. Porter JF, McKay G, Choy KH (1999) The prediction of sorption from a binary mixture of acidic dyes using single-and mixed isotherm variants of the ideal adsorbed solute theory. Chem Eng Sci 54:5863–5885
68. Amtul Q, Syed AK, Saeeda NA (2017) Equilibrium modelling for adsorption of aqueous Cd(II) onto turmeric: linear versus nonlinear regression analysis. Mor J Chem 2:362–370
69. Ho YS, Chiu WT, Wang CC (2005) Regression analysis for the sorption isotherms of basic dyes on sugarcane dust. Bioresour Technol 96:1285–1291
70. Husein DZ, Hassanien R, Al-Hakkani MF (2019) Green synthesized copper nano-adsorbent for the removal of pharmaceutical pollutants from real wastewater samples. Heliyon 5:e02339
71. Lee TZE, Zhang J, Feng Y, Lin X, Zhou J (2021) Adsorption of Cd (II) ions by coconut copra: isotherm and regeneration studies. IOP Conf Ser: Earth Environ Sci 657. https://doi.org/10.1088/1755-1315/657/1/012026
72. Dehghani MH, Dehghan A, Alidadi H et al (2017) Removal of methylene blue dye from aqueous solutions by a new chitosan/zeolite composite from shrimp waste: kinetic and equilibrium study. Korean J Chem Eng 34:1699–1707. https://doi.org/10.1007/s11814-017-0077-2
73. Naeem S, Baheti V, Wiener J, Marek J (2017) Removal of methylene blue from aqueous media using activated carbon web. J Text Inst 108:803–811. https://doi.org/10.1080/00405000.2016.1191745
74. Shakoor S, Nasar A (2016) Removal of methylene blue dye from artificially contaminated water using citrus limetta peel waste as a very low cost adsorbent. J Taiwan Inst Chem Eng 66:154–163. https://doi.org/10.1016/j.jtice.2016.06.009